Journal of Power Sources 195 (2010) 5138–5143

Contents lists available at ScienceDirect

Journal of Power Sources

journal homepage: www.elsevier.com/locate/jpowsour

Improved performance of dye-sensitized solar cells with TiO_2/alumina core–shell formation using atomic layer deposition

V. Ganapathy [1], B. Karunagaran [1], Shi-Woo Rhee *

System on Chip Chemical Process Research Center, Department of Chemical Engineering, Pohang University of Science and Technology (POSTECH), San 31 Hyoja-Dong, Nam-Ku, Pohang 790-784, South Korea

ARTICLE INFO

Article history:
Received 4 November 2009
Received in revised form
30 December 2009
Accepted 22 January 2010
Available online 10 February 2010

Keywords:
Atomic layer deposition
Core/shell nanoparticles
TiO_2–dye interface
Al_2O_3-coated TiO_2 electrodes
Dye-sensitized solar cells

ABSTRACT

Alumina (Al_2O_3) shell formation on TiO_2 core nanoparticles by atomic layer deposition (ALD) is studied to suppress the recombination of charge carriers generated in a dye-sensitized solar cell (DSSC). It is relatively easy to control the shell thickness using the ALD method by controlling the number of cycles. An optimum thickness can be identified, which allows tunneling of the forward current while suppressing recombination. High-resolution TEM measurements show that a uniform Al_2O_3 shell is formed around the TiO_2 core particles and elemental mapping of the porous TiO_2 layer reveals that the Al_2O_3 distribution is uniform throughout the layer. The amount of dye absorption is increased with increase in the shell thickness but electrochemical impedance spectroscopic (EIS) measurement shows a drastic increase in the resistance. With an optimum Al_2O_3 thickness of 2 nm deposited by ALD, a 35% improvement in the cell efficiency (from 6.2 to 8.4%) is achieved.

1. Introduction

Dye-sensitized solar cells (DSSCs) based on nanoporous TiO_2 electrodes are attracting world-wide interest as a promising way for the direct conversion of sunlight into electrical energy at a low cost and with promising efficiency [1]. In a DSSC, dye molecules are chemisorbed on a TiO_2 porous layer surface and visible light is absorbed by the sensitizer dye to generate excited electrons. Electron injection from the excited state of the dye into the conduction band of the TiO_2 is followed by the subsequent regeneration of the dye by an I^-/I_3^- redox couple. Efficient operation of a DSSC device relies on minimization of the possible recombination pathways occurring at the TiO_2|dye|electrolyte interface to allow efficient charge transport through the TiO_2 porous layer and subsequent charge collection at the device contacts. The energy band structure at the TiO_2|dye interface where charge separation processes take place in a DSSC with photon illumination is illustrated in Fig. 1. There are two possible recombination losses to consider. The photo-generated electrons may recombine either with oxidized dye molecules (process (3) in Fig. 1) or with the oxidized redox couple (process (5) in Fig. 1); the latter reaction is thought to be particularly critical to the device performance [2].

In order to reduce the recombination, many groups have proposed device architectures [2–10] that include the use of insulating polymers [3] and the use of very thin layered, high band-gap semiconductor metal oxides like ZnO and Nb_2O_5 [9–11]. Also the use of insulating metal oxides such as $CaCO_3$, $BaTiO_3$, MgO and Al_2O_3 between the TiO_2 and the dye interface has been attempted [2,7,8,12–14]. Al_2O_3 has been studied as an insulating barrier given its high conduction band edge compared with TiO_2. Moreover, the higher isoelectric point (IEP) of Al_2O_3 compared with TiO_2 favours more dye adsorption and thereby higher light absorption [8]. A comparison of the band gap and IEP of a few interesting shell materials is shown in Fig. 2; the data are taken from the literature mentioned above. Recently, Kim et al. [15] proposed that the open-circuit voltage (V_{oc}) is closely related to the conduction band edge position and the band-gap energy of the metal oxide shell layers, while the short-circuit current density (J_{sc}) is related to the IEP.

Although most of the TiO_2 surface modifications using an Al_2O_3 barrier layer have been based on the simple solution deposition method, precise control of the barrier thickness or conformal coating is not easy with this approach. Atomic layer deposition (ALD) is one alternative where precise control of the thickness and conformal coating is possible. ALD is an efficient process for controlling the nanostructure and layer thickness by regulating the number of deposition cycles. Photoelectrodes modified by ALD have been reported recently, where a very thin layer (~0.1 nm, approximately 1 cycle of ALD) of Al_2O_3 has been found to exhibit better performance than a bare sample [5,6]. Though the ALD process is a highly

* Corresponding author. Tel.: +82 54 279 2265; fax: +82 54 279 8619.
E-mail address: srhee@postech.ac.kr (S.-W. Rhee).
[1] These authors have contributed equally to this work.

0378-7753/$ – see front matter © 2010 Elsevier B.V. All rights reserved.
doi:10.1016/j.jpowsour.2010.01.085

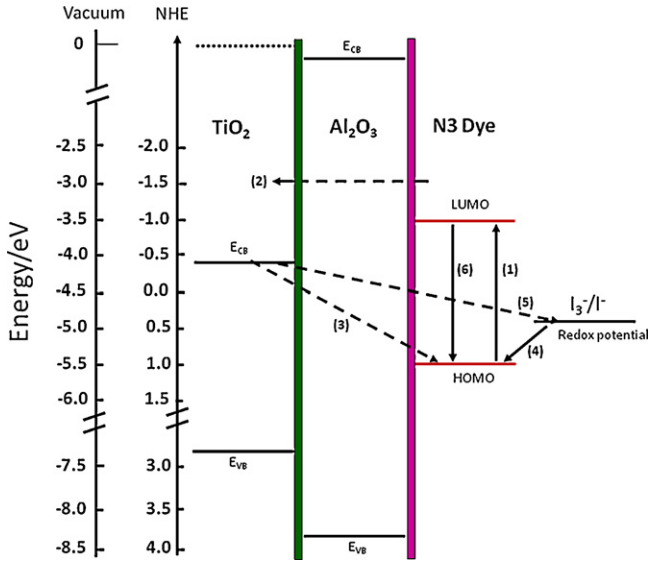

Fig. 1. Schematic diagram of band structure including interfacial charge-transfer processes occurring at TiO_2|dye|electrolyte interface in dye-sensitized solar cells.

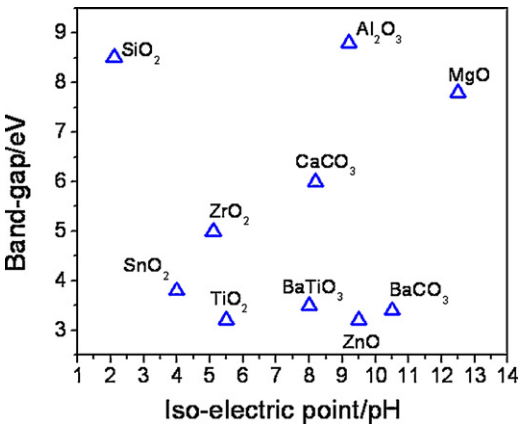

Fig. 2. Graphical representation of isoelectric point (basicity) and band gap of various oxide materials. Values are taken from available literature.

conformal coating method for a porous structure, a uniform coating is not likely to occur at such a low thickness. The ALD of Al_2O_3 is well established and with a number of cycles less than 10, an isolated island structure would be formed on TiO_2 surface. For more than 10 cycles, continuous films are likely to be formed to give a core–shell structure [16]. Other work reported the formation of Al_2O_3 barrier layer using d.c. magnetron sputtering. An approximately 12 nm thick layer of Al_2O_3 on TiO_2 was found to exhibit high efficiency, but this observation was not consistent with those in the available literature [4]. A wide range of thickness for the Al_2O_3 barrier layer or the shell layer, i.e., from 0.1 to 12 nm, have been reported for efficient DSSCs [2,4,12–14,17].

It is likely that there is an optimum thickness to reduce the recombination and at the same time to allow the electron flow from the dye to the TiO_2 layer without too much resistance. In the work reported here the effect of the barrier layer thickness on the device performance, is examined by forming an Al_2O_3 shell/TiO_2 core structure via the ALD process and analysis is carried out to study the nano structure, chemical composition, resistance, dye attachment and cell efficiency.

2. Experimental details

F:SnO_2 (FTO) glass plates (11 Ω/□, 2.3 mm thickness) were cleaned with a detergent solution in an ultrasonic bath for 20 min, followed by cleaning in DI (de-ionized) water and ethanol for 10 min each, then drying in a stream of nitrogen. A porous TiO_2 layer was prepared by applying a paste of TiO_2 nanoparticles (Ti-Nanoxide T20 from Solaronix) by means of a doctorblade on the FTO glass substrates and then annealing at 450 °C in air for 30 min. The thickness of the transparent electrode was approximately 9 μm and the active area of the cell was 0.25 cm^2. The TiO_2 photoelectrodes on the glass substrate were immediately transferred to a homemade ALD reactor and after sintering, Al_2O_3 was deposited using trimethylaluminum (TMA, Aldrich) as a metal precursor and water as an oxygen precursor. Nitrogen was used as a carrier gas and Al_2O_3 was grown at 150 °C using reactant exposure times of 1 s for both precursors and nitrogen purge times of 10 s between exposures. Thicker layers (20–200 nm) were grown to measure the growth rate, which was about 0.11 nm per cycle, i.e., comparable with the data obtained by other authors [18–20].

The alumina thickness was controlled by varying the number of ALD cycles; in the present work 10, 20, 30 and 40 cycles were used along with a bare TiO_2 sample for comparison. The alumina-coated TiO_2 electrodes were immediately immersed in a 0.3 mM solution of 'N3' dye in ethanol for 24 h. After removal from the dye solution, the treated electrode was washed with ethanol and dried in a stream of high-purity nitrogen. A 60-μm thick surlyn spacer (SX1170-60 from Solaronix) was sandwiched between the photoelectrode and a platinum-coated FTO counter electrode. An iodide based electrolyte (AN 50 from Solaronix) was used as a redox couple. The thickness of the nanocrystalline TiO_2 films was measured with a DEKTAK profilometer. Absorption spectra were recorded with a JASCO V-530 UV-Vis spectrometer. An FE-SEM (field emission scanning electron microscope) coupled with an EDX (energy dispersive X-ray spectrometer) was employed to study the morphological images and for composition analysis. An HR-TEM (high-resolution transmission electron microscope) was employed to determine the overcoat (alumina) thickness and the average particle size. The alumina thickness was also verified using spectroscopic ellipsometry with alumina deposited on a silicon substrate. X-ray photoelectron spectroscopy (XPS) measurements were employed to confirm the formation of alumina. Photovoltaic measurements employed an AM 1.5 solar simulator equipped with a 300 W xenon lamp (Newport, USA). The power of the simulated light was calibrated to 100 mW cm^{-2} by using a standard reference silicon solar cell (PV Measurement Inc.). Current–voltage (I–V) curves were obtained by applying an external bias to the cell and measuring the generated photocurrent with a Keithley model 2400 digital source meter. Electrochemical impedance spectroscope (EIS) measurements were carried out at room temperature in the frequency range of 100 mHz to 100 kHz at open-circuit voltage with a potential pulse of 10 mV in amplitude. Electrochemical parameters were derived from a.c. impedance spectra by using 'Zsimpwin' impedance analysis software.

3. Results and discussion

The SEM images of the surface morphology of alumina-coated TiO_2 in Fig. 3 clearly show a gradual increase in particle size with increase in ALD cycles. This confirms the formation of an alumina shell on top of the TiO_2 core particles. To check the distribution of Al_2O_3, EDX analysis was conducted for all the samples, the spectra are shown in Fig. 4a–d. Fig. 4a presents the EDX spectrum of the bare TiO_2 sample with Ti and O peaks. For the samples with an alumina shell layer, an additional Al peak is observed as shown in Fig. 4b–d. With increase in the number of deposition cycles, the Al content is increased. The remaining unassigned peaks arise from the substrate

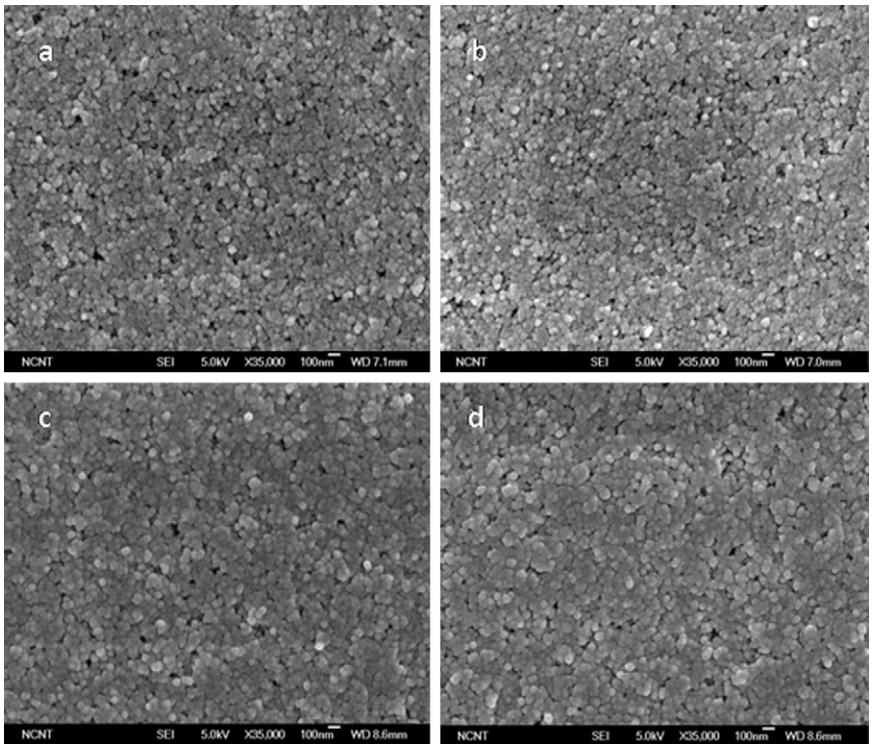

Fig. 3. FE-SEM surface morphological images showing growth of particle size with ALD cycles: (a) bare TiO_2, (b) 10 cycles, (c) 20 cycles and (d) 30 cycles. Scale bar = 100 nm.

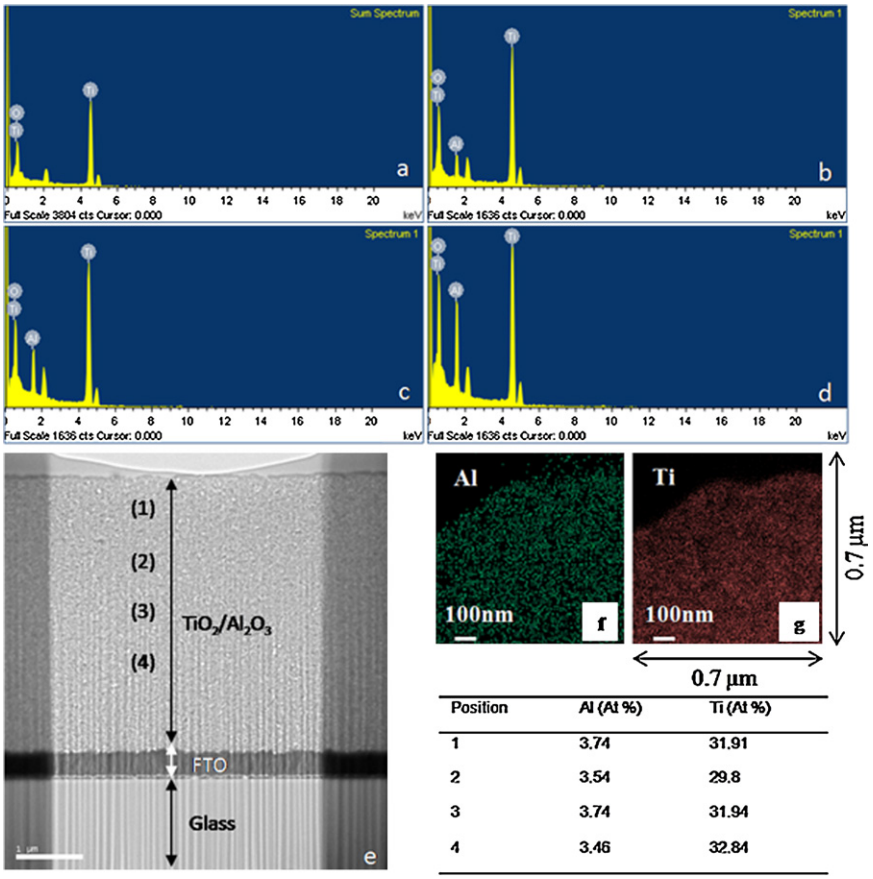

Position	Al (At %)	Ti (At %)
1	3.74	31.91
2	3.54	29.8
3	3.74	31.94
4	3.46	32.84

Fig. 4. Surface EDX spectra of (a) bare TiO_2, (b) 10 cycles, (c) 20 cycles and (d) 30 cycles alumina-coated sample. (e) Cross-sectional image of 20 cycles alumina-coated porous TiO_2 film deposited on FTO glass substrate (scale bar = 1 μm, TiO_2 layer thickness of 4 μm). EDX elemental mapping acquired by STEM, where distribution of Al and Ti atoms are given in (f) and (g), respectively. Table shows EDX results at different positions mentioned in (e).

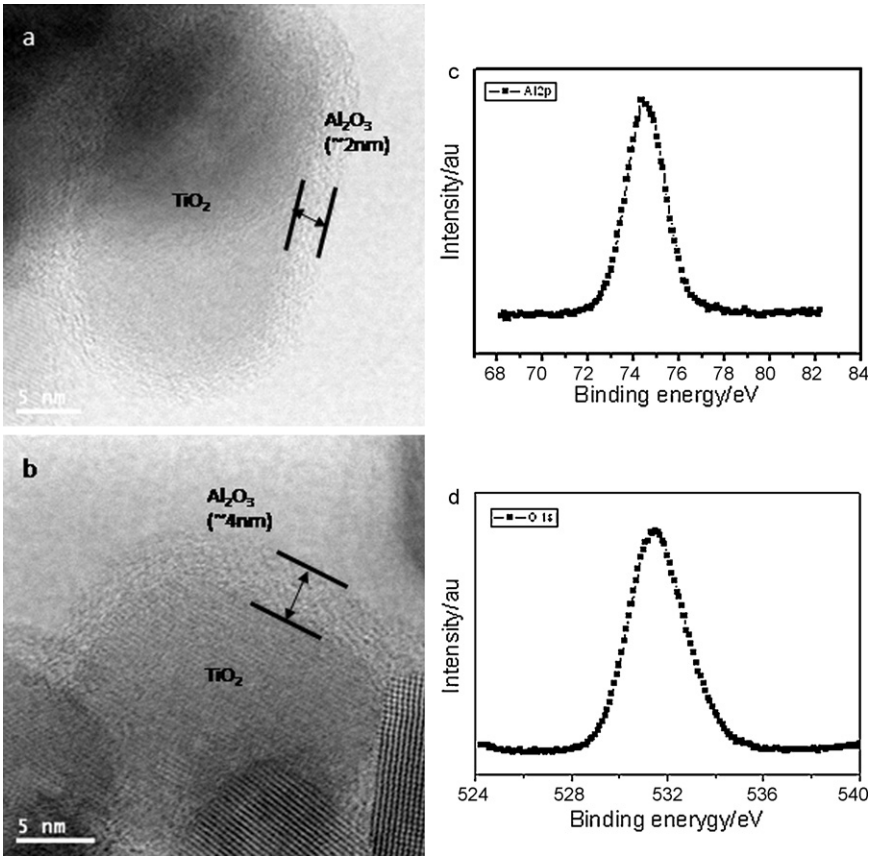

Fig. 5. HR-TEM images of TiO_2 porous layer covered with ALD alumina deposited with (a) 20 cycles and (b) 40 cycles. (c) and (d) show XPS spectra of Al2p and O1s core levels of 20 cycles sample.

and also from the transparent conducting oxide layer. The uniformity of the alumina deposition deep inside the TiO_2 nanoporous layer was confirmed for the ALD sample subjected to 20 cycles. For this measurement, the cross-section of the sample was prepared by means of a focused ion beam (FIB) method and the image in Fig. 4e confirms the uniform coverage of alumina over TiO_2 with a constant Al/Ti ratio of about 0.114 ± 0.005. Elemental mapping of Al and Ti shown in Fig. 4f and g also demonstrates the uniform coverage of the alumina layer.

HR-TEM analysis shows the formation of the alumina layer over TiO_2 particle and its thickness. The magnified HR-TEM images of ALD samples after 20 and 40 cycles are given in Fig. 5a and b, respectively. These reveal the uniform shell formation around TiO_2 with an alumina layer thickness of ~2 nm at 20 cycles and ~4 nm at 40 cycles. The XPS core levels of Al2p and O1s are presented in Fig. 5c and d, respectively. XPS analysis further supports the formation of alumina on top of TiO_2. For this analysis, TiO_2 electrodes coated with 20 cycles of alumina have been chosen. The peaks of Al2p and O1s are observed at 74.4 and 531.5 eV, respectively. The peak positions of Al in Al_2O_3 and O in Al_2O_3 match those given in the XPS handbook [21]. The difference between these two elemental peaks is close to the standard literature values for different forms of aluminum oxide [22,23]. To determine the amount of dye absorbed on bare and alumina-coated TiO_2, the dyes were desorbed from TiO_2 photoelectrodes using 0.1 M NaOH and the absorbance of the solution was measured with a UV–vis spectroscope. The results show an improvement in dye absorption with increase in Al_2O_3 layer thickness, as shown in Fig. 6. This is because the carboxylic acid groups in the dye react more favourably on a surface with a more basic nature or a higher IEP, such as Al_2O_3 (~9.5), than with anatase TiO_2 (~5.5). This leads to better light absorption [8,24] and core–shell materials with larger differences in the value of IEP (for TiO_2–Al_2O_3, the IEP difference is high) results in larger J_{sc}.

In order to determine the charge-transfer resistance between the transparent conducting oxide (FTO) and the TiO_2 porous layer and the interface between $TiO_2|Al_2O_3|$dye/electrolyte, the impedance of the cells was measured at open-circuit voltage under dark conditions with electrochemical impedance spectroscope (EIS), as shown in Fig. 7. The measured frequency range was from 0.1 Hz to 100 kHz. Usually, the impedance plot of a DSSC exhibits two or three arcs or semicircles in the Nyquist diagram

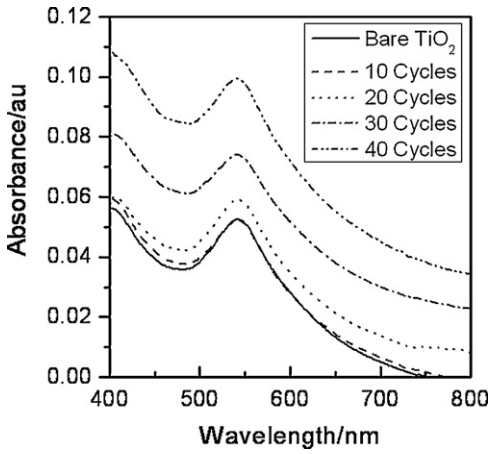

Fig. 6. Absorbance spectra of dye desorbed from bare and alumina-coated TiO_2 samples using 0.1 M NaOH. Alumina deposited with ALD process with number of deposition cycles between 10 and 40.

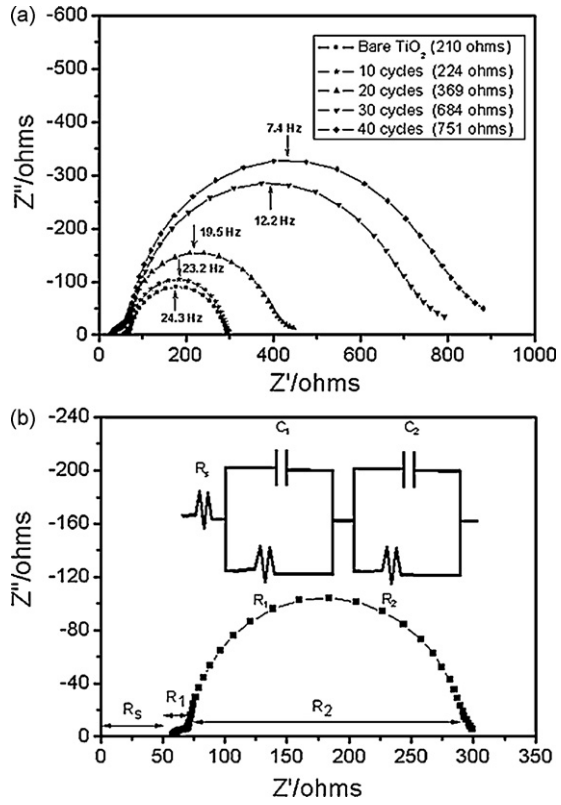

Fig. 7. (a) Impedance plot of bare and alumina-coated samples with TiO_2|dye|electrolyte interface resistance value is given in inset. Alumina deposited with ALD process with number of deposition cycles between 10 and 40 and maximum frequency corresponding to each semicircle is given. (b) Measured impedance data (solid symbol) and calculated impedance data (solid line) for 10 cycles sample. Equivalent-circuit model used for simulation is given in inset.

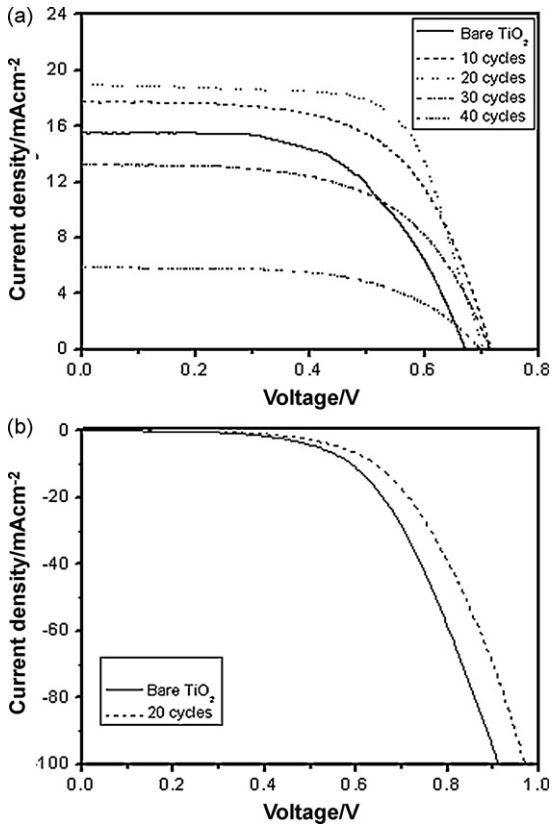

Fig. 8. (a) Current–voltage (*I–V*) characteristics of solar cell with bare and alumina-coated TiO_2 samples measured under one sun illumination. Alumina deposited with ALD process with number of deposition cycles between 10 and 40. (b) *I–V* curve of bare TiO_2 and 20 cycles alumina-coated sample measured in dark.

[25,26]. Each semicircle can be assigned based on model circuits for DSSCs. The first semicircle, i.e., the one in the high-frequency region, is attributed to the impedance of the charge-transfer process at the counter electrode. The second semicircle, i.e., in the middle-frequency region, is related to the charge-transfer process at the TiO_2|dye|electrolyte interface as well as the resistance to the transport of electrons to the conduction electrode on the glass substrate. The third arc in the low-frequency region, is attributed to Nernstian diffusion in the electrolyte. Tail of the third arc becomes longer when the thickness of the electrolyte layer is increased by placing a counter electrode far from a working electrode. The EIS plots of the bare and alumina-coated samples have two semicircles, as shown in Fig. 7a. The one in the high-frequency region is assigned to the charge-transfer process at the counter electrode as mentioned above. The charge-transfer resistance at the counter electrode is almost the same (~15 Ω) for both bare and alumina-coated samples. The second arc denotes the resistance between the TiO_2|dye|electrolyte interface (R_k) and also the resistance for the transport of electrons to the conduction glass electrode (R_w) for the bare sample, and also the change in the interface resistance for the sample with Al_2O_3 between the TiO_2 and the dye. The shape of the central arc is a true semicircle; hence according to Bisquert [27] and Adachi et al. [28], R_k is much larger than R_w, so the main contribution to the central arc is from the TiO_2|dye|electrolyte interface (R_k). The slightly increased resistance for the samples after 10 and 20 cycles suggests that the coating of Al_2O_3 increases the surface resistance of the TiO_2 electrode and with further increase in alumina thickness (at 30 and 40 cycles); significant increase in the surface resistance of the TiO_2 electrode is observed. The interface resistance values mentioned in the inset of the impedance plot are estimated by simulating the impedance data with 'Zsimpwin' software from a model of the equivalent circuit for the cell. The measured impedance data agree well with the calculated data from the equivalent-circuit modelling for the cells, as shown in Fig. 7b.

Performance parameters of the solar cells made with bare TiO_2 electrodes and with Al_2O_3-coated electrodes were studied with a solar simulator under one sun illumination. The observed *I–V* curve is presented in Fig. 8a and the corresponding solar cell parameters are tabulated in Table 1. For a bare TiO_2 photoelectrode, an efficiency of 6.2% is achieved. With increase in the number of coating cycles, a large increase in J_{sc}, V_{oc} and the fill factor (FF), and thus in efficiency (η), is observed up to 20 cycles. The increase in photocurrent, and hence efficiency, is likely to arise from an increase in dye absorption and a reduction in carrier recombination. The improvement in photo-voltage is attributed to a reduction in dark current for the cells with alumina layers, as shown in Fig. 8b, and is in agreement with the results of other workers [5,29]. The Al_2O_3 layer has a higher conduction band edge and a higher band gap than TiO_2 and therefore acts as a blocking layer and suppresses the recombination of the injected electrons either with the oxi-

Table 1
Solar cell performance parameters of bare and alumina-coated TiO_2 samples measured using a solar simulator under one sun illumination (100 mW cm^{-2}).

Sample	J_{sc} (mA cm^{-2})	V_{oc} (mV)	FF	Efficiency (%)
Bare TiO_2	15.5	669.1	60	6.2
10 cycles	17.7	716.3	61	7.7
20 cycles	19	705.6	63	8.4
30 cycles	13.26	715	60	5.6
40 cycles	5.93	695	50	2.1

J_{sc}, short-circuit current; V_{oc}, open-circuit voltage; FF, fill factor (cell area = 0.25 cm^2).

dized dye molecules or with the oxidized redox couple. With the recombination of the injected electrons retarded, the electron population and the resulting quasi-Fermi level of TiO_2 nanoparticles near the metal oxide overlayer will increase. As a result, V_{oc} will increase due to the increased offset between the quasi-Fermi level of the TiO_2 and the redox level of the electrolytes. This is the blocking effect of the Al_2O_3 layer. The application of more than 20 ALD cycles yields only a small variation in V_{oc}. The photocurrent density, on the other hand, drops sharply as the coating thickness increases. This clearly reveals that the thickness of alumina has exceeded the tunnelling thickness (~2 nm) and thereby leads to a decrease in device performance. Though the amount of dye adsorption is higher in the thicker Al_2O_3 samples (with the number of cycles higher than 20), it results in poor cell performance because the thick alumina barrier layer blocks electron injection into TiO_2. In the case of 10 and 20 cycles, the increase in the amount of dye attached on porous layer is not substantial but the Al_2O_3 layer coating improves the current and other cell parameters by suppressing the electron recombination.

4. Conclusions

In summary, alumina modification of TiO_2 by ALD has been demonstrated as a means of increasing the efficiency of dye-sensitized solar cells. A layer of Al_2O_3 on TiO_2 surface reduces the loss of electrons by suppressing their recombination, and this results in a significant increase in the short-circuit current and the overall power conversion efficiency. The improvement is also obtained from enhancement of dye absorption on the alumina surface. It is confirmed that the optimum thickness of alumina on TiO_2 is about 2 nm for high-performance DSSCs. When, however, the thickness is higher than 2 nm, the resistance becomes too high and the layer blocks electron transfer from the dye to the TiO_2 layer.

Acknowledgment

This study was supported by the Korea Science and Engineering Foundation (KOSEF) through the National Research Laboratory Project, and the nano fusion program of the POSCO.

References

[1] B. Oregan, M. Grätzel, Nature 353 (1991) 737–740.
[2] E. Palomares, J.N. Clifford, S.A. Haque, T. Lutz, J.R. Durrant, Chem. Commun. (2002) 1464–1465.
[3] B.A. Gregg, F. Pichot, S. Ferrere, C.L. Fields, J. Phys. Chem. B 105 (2001) 1422–1429.
[4] S. Wu, H. Han, Q. Tai, J. Zhang, S. Xu, C. Zhou, Y. Yang, H. Hu, B. Chen, X.-Z. Zhao, J. Power Sources 182 (2008) 119–123.
[5] T.W. Hamann, O.K. Farha, J.T. Hupp, J. Phys. Chem. C 112 (2008) 19756–19764.
[6] C. Lin, F.-Yu. Tsai, M.-H. Lee, C.-H. Lee, Ta.-C. Tien, L.-P. Wang, S.-Y. Tsai, J. Mater. Chem. 19 (2009) 2999–3003.
[7] J.R. Durrant, S.A. Haque, E. Palomares, Coord. Chem. Rev. 248 (2004) 1247–1257.
[8] E. Palomares, J.N. Clifford, S.A. Haque, T. Lutz, J.R. Durrant, J. Am. Chem. Soc. 125 (2003) 475–482.
[9] A. Zaban, S.G. Chen, S. Chappel, B.A. Gregg, Chem. Commun. (2000) 2231–2232.
[10] N.G. Park, M.G. Kang, K.M. Kim, K.S. Ryu, S.H. Chang, Langmuir 20 (2004) 4246–4253.
[11] K.E. Kim, S.R. Jang, J. Park, R. Vittal, K.J. Kim, Sol. Energy Mater. Sol. Cells 91 (2007) 366–370.
[12] Z.S. Wang, M. Yanagida, K. Sayama, H. Sugihara, Chem. Mater. 18 (2006) 2912–2916.
[13] S. Lee, J.Y. Kim, K.S. Hong, H.S. Jung, J.K. Lee, H. Shin, Sol. Energy Mater. Sol. Cells 90 (2006) 2405–2412.
[14] L. Zhang, Y. Shi, S. Peng, J. Liang, Z. Tao, J. Chen, J. Photochem. Photobiol. A: Chem. 197 (2008) 260–265.
[15] J.Y. Kim, S. Lee, J.H. Noh, H.S. Jung, K.S. Hong, J. Electroceram. 23 (2009) 422–425.
[16] K. Grigoras, S. Franssila, V.-M. Airaksinen, Thin Solid Films 516 (2008) 5551–5556.
[17] G.R.R.A. Kumara, K. Tennakone, V.P.S. Perera, A. Konno, S. Kaneko, M. Okuya, J. Phys. D: Appl. Phys. 34 (2001) 868–873.
[18] A.W. Ott, J.W. Klaus, J.M. Johnson, S.M. George, Thin Solid Films 292 (1997) 135–144.
[19] R.L. Puurunen, W.F.A. Besling, O. Richard, H. Bender, T. Conard, Ch. Zhao, A. Delabie, M. Caymax, S. de Gendt, M. Heyns, M.M. Viitanen, M. de Ridder, H. Brongersma, Y. Tamminga, T. Dao, T. de Win, M. Verheijen, M. Kaiser, M. Tuominen, J. Appl. Phys. 96 (2004) 4878–4889.
[20] S.-Ch. Ha, E. Choi, S.-H. Kim, J.S. Roh, Thin Solid Films 476 (2005) 252–257.
[21] J.F. Moulder, Hand Book of X-ray Photoelectron Spectroscopy, Perkin Elmer Corporation, 1992.
[22] E. Ghiraldelli, C. Pelosi, E. Gombia, G. Chiavarotti, L. Vanzetti, Thin Solid Films 517 (2008) 434–436.
[23] O. Bose, E. Kemnitz, A. Lippitz, W.E.S. Unger, Fresen. J. Anal. Chem. 358 (1997) 175–179.
[24] P. Qu, G.J. Meyer, Langmuir 17 (2001) 6720–6728.
[25] J. Van de Lagemaat, N.G. Park, A.J. Frank, J. Phys. Chem. B 104 (2000) 2044.
[26] Q. Wang, J. Moser, M. Gratzel, J. Phys. Chem. B 109 (2005) 14945–14953.
[27] J. Bisquert, J. Phys. Chem. B 106 (2002) 325.
[28] M. Adachi, M. Sakamoto, J. Jiu, Y. Ogata, S. Isoda, J. Phys. Chem. B 110 (2006) 13872–13880.
[29] A. Kay, M. Gratzel, Chem. Mater. 14 (2002) 2930–2935.